Science, Engineering & Education,8, (1), 2023, 36-42

Model-Based Approach for Analysis of Contrast Media Regions in Contrast Enhanced Breast Model Images

Tihomir Georgiev[1]*, Elena Koleva[2,3]

[1]Medical University of Varna, 55 Marin Drinov Str, Varna 9002, Bulgaria
[2]University of Chemical Technology and Metallurgy, 8 Kliment Ohridski Blvd., Sofia 1797, Bulgaria
[3]Institute of Electronics, Bulgarian Academy of Sciences, 72 "Tzarigradsko Chaussee blvd", 1784 Sofia, Bulgaria

Received 30 June 2023, Accepted 10 September 2023

ABSTRACT

Contrast agents in radiology improve visualisation and iodine-based ones are applied in different radiology techniques. Energies, used in these techniques, vary in a very wide range. The energies can be as low as 26 kVp in mammography and reach up to 140 - 150 kVp in computed tomography. Dual-energy studies can also be applied. X-ray images of resin phantoms with iodine-based contrast base are taken at different energies and the image pixel values of various regions of interest were measured. Based on the performed measurements, the visual contrast between the studied different areas is calculated and analysed. The obtained data are applied for the estimation of models for the expected pixel values depending on the energies and the contrast agent quantities. These models can be used to describe the real conditions, which differ from the applicable to theoretical calculations ideal conditions.

Keywords: iodine-based contrast, radiology, X-ray image processing, breast cancer detection, model-based approach.

INTRODUCTION

The contrast in medical imaging is used to provide better visualisation. The iodine-based contrast agents have been used in computed tomography (CT) since many years. Typical energies for the CT are from 70 - 80 kVp up to 140-150 kVp [1, 2] and can be used in both conventional systems [2] and dual-energy studies [1]. The use of contrast agents is not only limited to CT. Breast cancer detection in early stages is of great importance but can be hindered by dense tissues. In order to avoid this, contrast agents can be used. Specialised mammography studies date back to 1960s, the ones that include contrast agents were introduced in 1970s and techniques of contrast-enhanced dual-energy mammography and single-energy temporal subtraction mammography were developed later [3 - 7].

The dose applied in contrast-enhanced dual-

**Correspondence to: Tihomir Georgiev, Medical University of Varna, 55 Marin Drinov, Varna 9002, Bulgaria, E-mail: t.georgiev@mu-varna.bg*

energy mammography is higher compared to the conventional mammography but the estimation of how much higher varies. In [4] it was considered that the doses are higher in the range 20 - 50 % than the conventional, while others state approximately 20 % [7 - 9] higher doses. The lower energy settings in contrast enhanced dual-energy mammography are typically in the range of 26 - 33 kVp and the higher energy settings are in the range of 44 - 50 kVp [6 - 9].

In this study we analysed X-ray images of iodine-based contrast agent in 10 pits in resin phantom taken at different energies. Based on the performed measurements in several regions of interest (RoI), the visual contrast between the studied different areas is calculated and analysed. The obtained data are applied for the estimation of models for the expected pixel values depending on the energies and the contrast agent quantities. These models can be used to describe the real conditions, which differ from the applicable to theoretical calculations ideal conditions.

EXPERIMENTAL

Five X-ray images of a phantom, printed with Formlabs Clear resin and filled with the commercially available iohexol-based contrast agent, were used in the current study. 10 pits on top of the phantom with depths from 0.1 mm to 1.0 mm are filled with the contrast agent and irradiated with different energies. Detailed modelling, materials selection with resin similarity to soft tissues, phantom printing, X-ray imaging and images themselves as well as calculation kVp to keV, including the approximation of the used in the study energy range 50 kVp - 120 kVp with 32 keV - 49 keV were reported previously in [10 - 12].

Regions of interest (RoI) were assigned on the images (Fig. 1) - one RoI for each pit at each energy and five RoI between the contrast object rows at each energy. The correspondence in the notations in Fig. 1 is the following: 1 - 1.0 mm, 2 - 0.9 mm, 3 - 0.8 mm, etc.

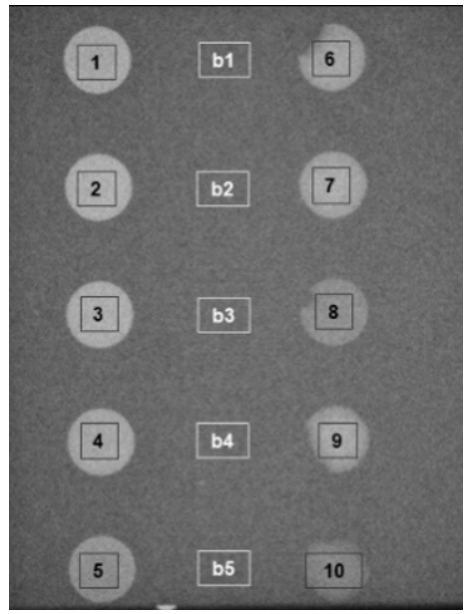

Fig. 1. Regions of interest (RoI) - for each pit with iohexol-based contrast agent at each energy and five background RoI between the contrast object rows.

The mean (p_m) and the standard deviation (s_p) of the pixel values in each RoI were measured using ImageJ [13]. The obtained results are presented in Table 1.

RESULTS AND DISCUSSION

Theoretical visual contrast modelling

Lambert's law provides relation between light intensities of the incident beam, transmitted radiation, pathlength and the absorption coefficient of the medium [14]. In the described study, two formulae are used:

• background:

$$\frac{I_1}{I_0} = e^{-\mu_1 d_1}$$

• iohexol-based contrast agent:

$$\frac{I_2}{I_0} = e^{-[\mu_1 (d_1 - d) + \mu_2 d]}$$

where μ_1 and μ_2 are the attenuation coefficients correspondingly for the resin and the iohexol-

Table 1. RoI mean and standard deviation of pixel values for different energies.

E	50 kVp		70 kVp		80 kVp		100 kVp		120 kVp	
d*	p_m	s_p	p_m	s_p	p_m	s_p	p_m	s_p	p_m	s_p
1.0	2637	123	2136	61.1	2064	60.7	2049	68.4	1968	63.8
0.9	2808	125	2294	47.6	2214	48.3	2206	64.9	2100	52.6
0.8	2805	112	2288	55.3	2214	44.3	2198	62.6	2092	45.7
0.7	2661	127	2165	57.9	2091	52.6	2088	66.9	1990	57.9
0.6	2255	116	1834	69.7	1783	65.6	1796	63.5	1720	59.9
0.5	2664	123	2151	62.1	2065	59.5	2092	66.6	1994	64.5
0.4	2771	129	2254	57.1	2183	51.5	2185	63.8	2082	46.9
0.3	2337	128	1912	64.9	1870	63.5	1898	67.9	1839	58.8
0.2	2732	122	2233	56.9	2155	54.5	2151	69.2	2043	62.1
0.1	2162	128	1769	69.2	1742	72.1	1758	75.3	1705	70.1
b1	1673	130	1399	73.5	1436	69.6	1495	65.9	1485	62.2
b2	1782	136	1494	68.6	1508	74.9	1544	63.2	1552	58.4
b3	1765	131	1514	64.5	1534	67.9	1573	71.8	1573	57.6
b4	1780	132	1501	64.1	1513	65.1	1529	69.4	1541	64.1
b5	1619	126	1383	81.4	1404	72.5	1493	66.3	1422	72.1

**d – pit depth, b – background (Fig. 1)*

based contrast agent, d_1 is the thicknesses of the phantom and d is the depth of the pit with contrast agent. I_0 is the intensity of the incident beam at the top of the phantom, and I_1 and I_2 are the intensities of the beam after passing through the phantom, respectively, for the resin (I_1) and pits with contrast agent (I_2).

Theoretical calculations for attenuation were performed using data from the NIST XCOM database [15], and materials approximations based on [16] for the iohexol-based contrast agent and [17] for the resin.

Regression models for the contrast agent attenuation (μ_2, mm^{-1}) and for the resin background attenuation (μ_1, mm^{-1}) were estimated based on the available reference data. They are presented in Table 2, together with their determination coefficients R^2. The attenuation of the contrast agent was approximated with two separate regression equations due to the iodine K-edge at 33.2 keV ($\hat{\mu}_{21}, \hat{\mu}_{22}$). In the estimated models E_{keV} is the energy in keV.

Energy in kVp (E_{kVp}) equivalence to E_{keV} was calculated using TASMIP Spectra calculator [18].

The Weber contrast [19] is calculated by:

$$C_w = \frac{I_2 - I_1}{I_1} = \frac{e^{-[\mu_1(d_1-d)+\mu_2 d]}}{e^{-\mu_1 d_1}} - 1$$

The estimated theoretical model of C_w, depending on E_{kVp} and d is presented graphically on the contour plot in Fig. 2.

Empirical visual contrast modelling

The visual contrast for every pit and at every energy was calculated using the formula:

$$C_w = \frac{I_2 - I_1}{I_1} = \frac{I_2}{I_1} - 1.$$

The ratio between intensities was calculated by the ratio between the mean pixel values of the RoI.

Regression models for p_m and s_p of the pit area pixel values as functions of E_{kVp} and d are

Table 2. Attenuation regression models.

Energy region, keV	Material	Regression model	R^2, %
20 – 33.2	Iodine – based agent	$\hat{\mu}_{21} = 7.458 - 0.6251\ E_{keV} + 0.018714\ E_{keV}^2 - 0.000194\ E_{keV}^3$	99.99
33.2 – 70	Iodine – based agent	$\hat{\mu}_{22} = 7.385 - 0.31962\ E_{keV} + 0.004923\ E_{keV}^2 - 0.000026\ E_{keV}^3$	99.94
20 – 70	Resin	$\hat{\mu}_1 = \exp(1.2975 - 0.23862\ E_{keV} + 0.003909\ E_{keV}^2 - 0.000022\ E_{keV}^3)$	99.93

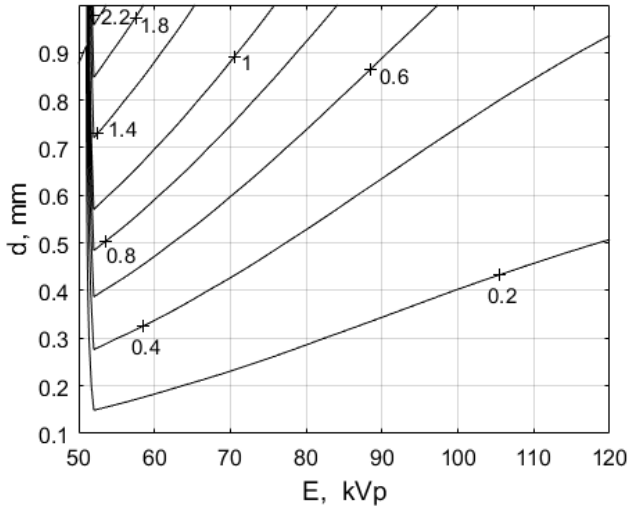

Fig. 2. Contour plot of the theoretical visual contrast Cw, depending on the energy E [kVp] and the pits depth d [mm].

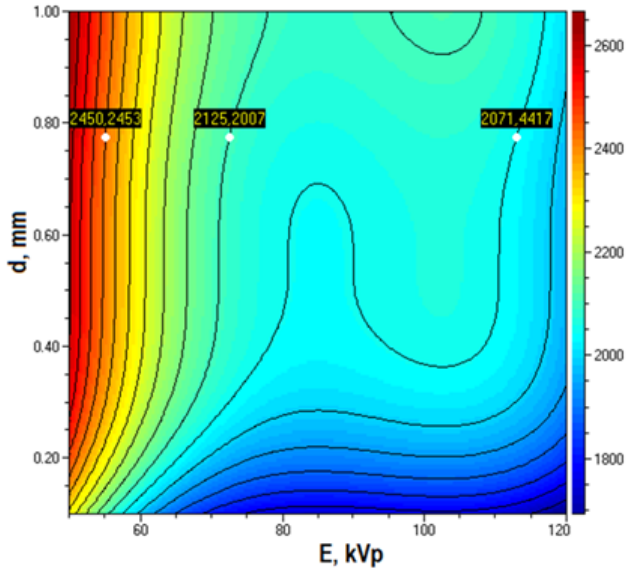

Fig. 3. Contour plot of the mean pixel values ($\hat{p}_m$) at the pit area.

presented in Table 3 along with the corresponding determination coefficients R^2. The models are given for dimensionless and coded in the region [-1 - 1] factors and denoted as: energy - x_1, pit depth – x_2. The relation between the natural and the coded (x_i) factor values can be done by:

$$x_1 = (E_{kVp} - 85)/35,\ x_2 = (d - 0.55)/0.45.$$

The contour plots of $\hat{p}_m$ and $\hat{s}_p$ for pit areas are shown in Fig. 3 and Fig. 4. Both the highest pixel values and the highest standard deviation values are at the lowest energies. At these energies the pit depths have small influence, if any.

Estimated models for $\hat{p}_m$ and $\hat{s}_p$ of the background are shown in Table 3 along with the corresponding determination coefficients R^2.

The empirical visual contrast model is presented graphically on the contour plot in Fig. 5.

Analysis of variance (ANOVA)

Intensities and therefore pixel values of the images depend on energy and media. Due to the beam geometry the background RoI closer to the phantom edge are expected to have lower pixel values. Two-way ANOVA analysis confirms

Table 3. Regression models for the mean pixel values (pm) and the standard deviations (sp) of the pit area and the background pixel values.

Parameter	Regression model	R^2, %
Pit area $\hat{p}_m$	$2067.3644 + 237.68429x_1^2 - 315.41895x_1^3 + 171.02548x_2^3 - 125.51561x_2^4$	73.03
Pit area $\hat{s}_p$	$56.017447 + 16.485632x_1 - 4.3549091x_2 + 32.668748x_1^2 + 4.9090909x_2^2 - 49.009374x_1^3$	95.65
Background $\hat{p}_m$	$9.223\times10^{16}\exp(-0.6686\ E_{kVp}) + 1386\exp(0.0008122\ E_{kVp})$	92.81
Background $\hat{s}_p$	$4.42\times10^{-14}\exp(0.2849\ E_{kVp}) + 149.1\exp(-0.01332\ E_{kVp})$	91.82

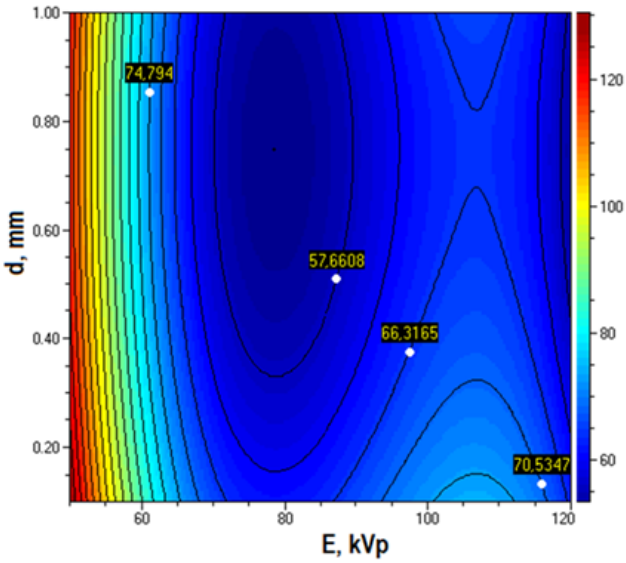

Fig. 4. Contour plot of the standard deviations ($\hat{s}_p$) of the pixel values at the pit area.

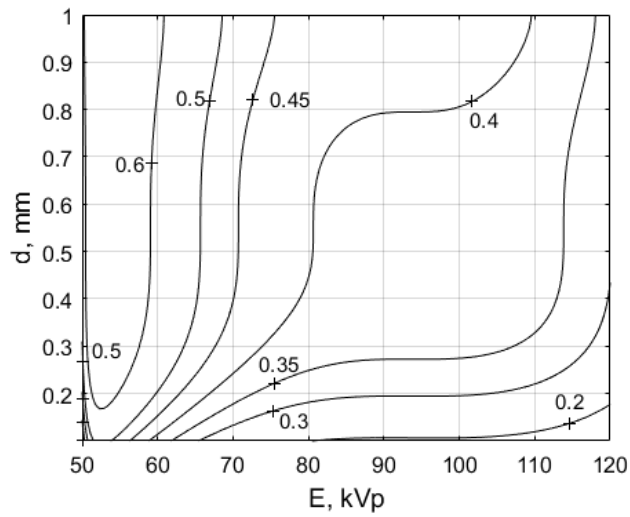

Fig. 5. Contour plot of the empirical visual contrast C_w, depending on the energy E [kVp] and the pits depth d [mm].

these dependencies. The largest pixel values are reached at energy 50 kVp, the differences of the means are not significant at 100 and 120 kVp, as well as at 70 and 80 kVp. The upper and the lower positions b1 and b5 differ significantly from the centre background pixel mean values.

Similarly, two-way ANOVA analysis confirmed dependency on the energy. The largest pixel values are reached at energy 50 kVp. All the differences of the pixel means at different energies are significant. There is no significant difference of the pixel means for some contrast agent thicknesses. Moreover, the expected change of systematic increase of the mean pixel value with the increase of the contrast agent pit depth is not observed. Therefore, these results are not only due to the distance to the phantom edge but are most likely influence also by the filling level.

CONCLUSIONS

The models, based on theoretical dependencies and experimental measurements, indicate several important points. Coefficients of determination of the empirical models for standard deviations of the contrast and background, and background pixel values are close to 1. The coefficient of determination of the empirical model for pit areas pixel values is not so high. The empirical model for the pit areas is close to the theoretical model only for the small depth pits and energies in the range at and above 70 kVp. Further, the estimated models suggested that the visual contrasts achieved with a contrast agent were relatively small $C_{w,min}$ = 0.7465 for the real images obtained with automated exposure control. The maximal theoretical value for the visual contrast is $C_{w,max}$ = 2.36 and might not be high enough for small objects.

Some of the sources for the differences between real and theoretical results, such as the materials properties, beam geometry, device specifics, and noises, were already reported in [12]. Calculations for the estimation of E_{kVp} to E_{keV} also have certain approximations.

The estimated models, based on the real images data, are a basis for a better description of the real situation than the theoretical models, which are relevant in ideal conditions. The models can be used for contrast-enhanced technique results prediction or after further development may be used for optimisation of the dual energy settings.

Acknowledgements

Participation of Tihomir Georgiev was supported by the European Union's Horizon 2020 research and innovation programme under the Marie Skłodowska-Curie grant agreement No. 101008020.

REFERENCES

1. A. Zegadło, M. Żabicka, A. Różyk, E. Więsik-Szewczyk, A new outlook on the ability to accumulate an iodine contrast agent in solid lung tumors based on virtual monochromatic images in dual energy computed tomography (DECT): Analysis in two phases of contrast enhancement, J. Clin. Med., 10, (9), 2021, 1870.
2. M.-H. Choi, Y.-J. Lee, S.-E. Jung, The image quality and diagnostic performance of CT with low-concentration iodine contrast (240 mg Iodine/mL) for the abdominal organs, Diagnostics, 12, (3), 2022, 752.
3. P. Baldelli, A. Bravin, C. di Maggio, G. Gennaro, A. Sarnelli, A. Taibi, M. Gambaccini, Evaluation of the minimum iodine concentration for contrast-enhanced subtraction mammography. Phys. in Med. & Biology, 51, 2006, 4233-4251.
4. C. Dromain, C. Balleyguier, G. Adler, J. R. Garbay, and S. Delaloge, Contrast-enhanced digital mammography, Euro. J. of Radiology, 69, (1), 2009, 34-42.
5. A. Contillo, G. Di Domenico, P. Cardarelli, M. Gambaccini, A. Taibi, A novel approach to background subtraction in contrast-enhanced dual-energy digital mammography with commercially available mammography devices: Polychromaticity correction, Med. Phys., 42, (11), 2015, 6641-6650.
6. L. Nicosia, G. Gnocchi, I. Gorini, M. Venturini, F. Fontana, F. Pesapane, I. Abiuso, A.C. Bozzini, M. Pizzamiglio, A. Latronico, et al., History of mammography: Analysis of breast imaging diagnostic achievements over the last century. Healthcare, 11, (11), 2023, 1596.
7. R. Fusco, A. Piccirillo, M. Sansone, V. Granata, M.R. Rubulotta, T. Petrosino, M.L. Barretta, P. Vallone, R. Di Giacomo, E. Esposito, M. Di Bonito, A. Petrillo, Radiomics and artificial intelligence analysis with textural metrics extracted by contrast-enhanced mammography in the breast lesions classification, Diagnostics (Basel), 11, (5), 2021, 815.
8. J.S. Sung, L. Lebron, D. Keating, D. D'Alessio, C.E. Comstock, C.H. Lee, M.C. Pike, M.

Ayhan, C.S. Moskowitz, E.A. Morris, M.S. Jochelson, Performance of dual-energy contrast-enhanced digital mammography for screening women at increased risk of breast cancer, Radiology, 293, (1), 2019, 81-88.

9. A. Lorek, K. Steinhof-Radwańska, A. Barczyk-Gutkowska, W. Zarębski, P. Paleń, K. Szyluk, J. Lorek, A. Grażyńska, P. Niemiec, I. Gisterek, The usefulness of spectral mammography in surgical planning of breast cancer treatment-analysis of 999 patients with primary operable breast cancer, Curr. Oncol., 28, (4), 2021, 2548-2559.
10. T. Georgiev, K. Bliznakova, Contrast agent dual energy imaging: Computer simulations in search for printing materials, 2021 International Conference on e-Health and Bioengineering (EHB), Iasi, Romania: IEEE, 2021, pp. 1-4.
11. T. Georgiev, K. Bliznakova, Y. Baneva, A Method for Modelling of Contrast Enhanced Mammography Imaging: A Simulation Study, Bulg. J. of Publ. Health, 13, (4), 2021, 20-27.
12. T. Georgiev, N. Dukov, T. Todorov, K. Bliznakova, Contrast Enhanced Radiography with a Printed Model, 2022 E-Health and Bioengineering Conference (EHB), Iasi, Romania, IEEE, 2022, 1-4.
13. ImageJ: https://imagej.net/ij/index.html
14. I. Oshina, J. Spigulis, Beer-Lambert law for optical tissue diagnostics: current state of the art and the main limitations, J .Biomed. Opt., 26, (10), 2021, 100901.
15. NIST XCOM: Element/Compound/Mixture: https://physics.nist.gov/PhysRefData/Xcom/html/xcom1.html
16. OMNIPAQUE™ (iohexol) Injection, Reference ID: 4080358, General Electric Company, 2017.
17. PubChem, Epoxy resin": https://pubchem.ncbi.nlm.nih.gov/compound/169944
18. TASMIP Spectra Calculator - Calculate X-ray Imaging Spectra: http://solutioinsilico.com/medical-physics/applications/tasmip-app.php?ans=1&n_sp=1&k1=120&m1=13&t1=0.7&k2=&m2=1&t2=&k3=&m3=1&t3=
19. A. Beghdadi, On Measures of Visual Contrast and Their Use in Image Processing (invited paper), Colour and Visual Computing Symposium, 2020.